Environmental Science Advances

ROYAL SOCIETY OF CHEMISTRY

PAPER

View Article Online
View Journal | View Issue

Cite this: *Environ. Sci.: Adv.*, 2024, **3**, 1048

Water quality indicators influencing the formation and morphology of hydrostatically-formed photogranules†

Cynthia J. Castro, [ab] W. Camilla Kuo-Dahab, [a] Tao Jiang,[a] Sam Downes, [a] Guoping Zhang, [a] Ahmed S. Abouhend [a] and Caitlyn S. Butler *[a]

Received 13th February 2024
Accepted 8th May 2024

DOI: 10.1039/d4va00054d

rsc.li/esadvances

Hydrostatic photogranulation represents an intriguing phenomenon with potential applications in aeration-free wastewater treatment. In this process, activated sludge batches transform into photogranules, manifesting as either spherical or disk-dominated shapes. Yet, the factors contributing to this morphological diversity remain unknown. Moreover, the impact of morphology on granule structure and physical characteristics remains poorly understood, posing potential implications for photogranulation in reactors that frequently utilize these hydrostatic granules as seeding materials. This study investigates the influence of water quality parameters on hydrostatic photogranulation and its role in shaping granule morphology. Spherical photogranules exhibited lower chlorophyll *a* concentration (5.97–7.40 mg L^{-1}) and higher Chl *a*/*b* ratio (13–14) than disk-shaped photogranules (Chl *a* concentration: 8.13–11.70 mg L; *a*/*b* ratio: <10), indicating a higher cyanobacteria content in disk-shaped granules. Additionally, spherical photogranules showed significantly lower concentrations of EPS proteins and polysaccharides than disk-shaped granules, suggesting enhanced granulation under EPS limitations. Correlation analysis indicates that higher initial NO_3^- and total polysaccharides (TPS) increase the likelihood of producing spherical photogranules. Conversely, higher initial Ca^{2+} and Mg^{2+} concentrations were observed in cultivations predominantly producing disks. Furthermore, principal component analysis identified Cl^-, Na^+, NH_4^+, and SO_4^{2-} as key initial water quality indicators and TPS, tCOD, and VSS as important sludge biomass characteristics that distinguished between different photogranule morphologies. Compared to spherical photogranules, disk-dominated photogranules exhibited higher stiffness and shear resistance, potentially due to increased cyanobacterial and EPS contents. Controlling hydrostatic photogranulation to achieve desired photogranule shapes holds potential for customizing seed granules and thus enhancing the OPG wastewater treatment performance.

Environmental significance

This study unveils the opportunity to optimize the startup of the oxygenic photogranule (OPG) process by intentionally shaping seed hydrostatic photogranules. By discerning the impact of water quality on granule morphology, we present practical strategies to steer hydrostatic granulation towards enhanced reactor performance by attaining the desired photogranule shape. These insights pave the way for advancing the OPG process as an energy-efficient and sustainable wastewater treatment solution. By leveraging tailored approaches to granule formation, we can improve nutrient removal, enhance granule stability, and ultimately contribute to more effective and environmentally sound water treatment practices.

1. Introduction

Oxygenic photogranules (OPGs) are spherical aggregates composed of phototrophic and non-phototrophic microorganisms.[1–4] OPGs offer a unique approach to wastewater treatment by functioning without the need for mechanical aeration, which is currently the most energy-intensive process in wastewater treatment operations.[2,5–7] OPGs achieve wastewater treatment through a synergistic combination of biological and physical processes facilitated by their diverse microbial community.[1,2,6] The phototrophic microorganisms with OPGs, such as cyanobacteria and green algae, utilize sunlight in photosynthesis to produce oxygen as a byproduct, improving dissolved oxygen levels in the wastewater.[8] This oxygenation supports aerobic microbial activities, including organic matter degradation and pollutant transformation. OPGs also harbor anaerobic zones within their

[a]*University of Massachusetts Amherst, Department of Civil & Environmental Engineering, 18 Marston Hall, 130 Natural Resources Road, Amherst, MA, 01003, USA. E-mail: csbutler@umass.edu*

[b]*Wade Trim, 201 N Franklin St., Suite 1350, Tampa, FL 33602, USA*

† Electronic supplementary information (ESI) available. See DOI: https://doi.org/10.1039/d4va00054d

interior, promoting denitrification and other anaerobic processes for total nitrogen removal.[1,9] The formation of OPGs as a granular biofilm enhances microbial retention and metabolic activities, aiding in physical filtration and the decomposition of suspended solids. Additionally, phototrophic microorganisms uptake nutrients like nitrogen and phosphorus through bioassimilation, reducing nutrient loads in the wastewater.[10] Due to their larger size and density, OPGs can be easily separated from the bulk liquid after treatment without additional separation techniques.[2,11] This easily separated biomass can be utilized for downstream bioenergy generation processes.

According to the literature, OPGs can be generated under both hydrostatic conditions, which lack hydrodynamic shear, and under hydrodynamic conditions, where active mixing is employed.[1–3,6,7,12] Despite being produced in distinct environments, hydrostatic and hydrodynamic photogranules exhibit striking similarities in morphology, internal structure, and microbial composition.[1,2,13] Both types of granules are predominantly composed of filamentous and motile cyanobacteria belonging to the order Oscillatoriales, showcasing a layered structure where filamentous cyanobacteria form the outer layer encapsulating the inner non-cyanobacterial biomass.[1,2,14] The primary distinguishing factor between these granule types is their size.[1,2,6,14] The production of hydrostatic photogranules involves the transformation of activated sludge batches into photogranules under hydrostatic batch conditions with the presence of light.[1–4,15] This transformation occurs through the enrichment of the phototrophic community within the sludge biomass, resulting in approximately 50% phototrophic content.[1,4] The complete transformation takes approximately 2−4 weeks, yielding hydrostatic photogranules with a diameter up to 20 mm.[1,4]

Photogranulation under hydrodynamic conditions, *i.e.*, in wastewater treatment systems, involves several methods,[16–21] one of which is seeding hydrostatically formed granules in reactors with active mixing.[2,5,7,13,14] When using hydrostatic photogranules as seeds, the hydrodynamic shear within the reactors causes these granules to disintegrate, releasing aggregates smaller than 100 μm in diameter that gradually develop into mature photogranules over time.[1,2,7] Additionally, various types of seed biomass have been explored, including mixed cultures such as activated sludge with microalgal/cyanobacterial biofilm, aerobic granular sludge with unicellular green algae, or a combination of aerobic granular sludge and algae-bacterial granules.[16–21]

Seeding OPG reactors with hydrostatic granules or other types of reported phototrophic inoculums helps accelerate the process startup by promptly establishing a resilient microbial community, which facilitates a rapid transition to peak operational capabilities.[2,7] However, utilizing different seed sources has resulted in the development of photogranules with diverse structures, microbial compositions, and sizes.[1,3,13,16–20] When comparing various seeding methods, hydrostatic photogranules stand out for their well-defined characteristics and established production protocol, providing significant advantages in process reproducibility.[1,2,4] Thus, using hydrostatic OPGs for reactor seeding ensures a consistent starting point compared to other seeds that lack well-defined characteristics and reproducibility protocols for the seed biomass.

It has been reported in multiple studies that hydrostatic cultivation of various sludge types, and sometimes even the same sludge biomass, undergoes contraction and compaction, leading to the formation of two distinct morphologies: disk and spherical granules.[1,4,9,12] The disk morphology exhibits an ellipsoid shape with a filamentous outer layer, whereas the spherical granules appear with a smoother surface appearance.[1,4,9,12] Additionally, given that these granules often serve as the primary seed biomass for hydrodynamic growth, their influence on photogranulation within reactors may be different, particularly during the critical startup phase. This variation could be attributed to differences in the distribution of shear forces across the particle surface. Despite its importance, the prevalence of one morphology over another in a given cultivation set remains unclear. Moreover, there is a lack of comprehensive information regarding the distinct physical attributes that differentiate spherical and disk-shaped granules.

This study aims to explore the factors influencing the morphological outcomes of photogranules produced under hydrostatic conditions. The objective is to gain a deeper understanding of the relationship between the initial wastewater characteristics in the local environment and the success of OPG cultivation, defined as the formation of a spherical or disk-shaped photogranule. Specifically, the study seeks to establish correlations between initial water quality parameters and the resulting OPG morphology, distinguishing between spherical and disk granules, across cultivation sets. Additionally, this study investigates the influence of physical parameters in the local cultivation environment on the formation of hydrostatic OPGs. In-depth investigations into the structural integrity and mechanical strength of hydrostatic photogranules with different morphologies are conducted to offer nuanced insights into the physical variations of OPGs and their potential implications for performance in wastewater treatment.

2. Materials and methods

2.1. Hydrostatic photogranulation setup

Seven hydrostatic cultivations were conducted to produce OPGs. All cultivations followed a standardized preparation protocol. Briefly, activated sludge was collected and placed in a well-mixed, 2 L beaker. Aliquots of 10 mL of activated sludge were pipetted into 20 mL scintillation vials, capped, and placed under hydrostatic conditions.[1,4] Initial water quality parameters and sludge concentrations were measured for activated sludge and presented in Table 1. The vials were exposed to uniform illumination from LED lights (approximately 10 kLux) for 24 hours daily in a temperature-controlled room at 20 °C. The temperature and light intensity were measured at the side surface of each individual vial using a Lasergrip 774 Infrared Thermometer (Etekcity) and an EA30 EasyView Light Meter (Extech, FLIR Systems), respectively. After the final sampling day, a visual assessment of granule morphology was conducted for each vial within a cultivation set. Each cultivation had a range of formed photogranules (or remaining vials) at the end

Table 1 Summary data of initial water quality parameters and sludge concentrations of seven OPG cultivation sets[a]

		Am-100	Ha-100	Am-68.9 a	Ha-27.8	Am-17.1	Ha-14.3	Am-13.8 a
Chl *a*	(mg L^{-1})	0.416	0.315	2.04	0.341	0.510	1.10	1.24
Chl *b*	(mg L^{-1})	0.852	0.163	2.60	0.105	0.310	0.410	1.95
Chl *c*	(mg L^{-1})	1.18	0.171	3.17	0.055	0.184	0.171	2.35
VSS	(mg L^{-1})	1783	2810	1973	2343	1113	2793	1620
Chl *a*	(mg g^{-1} VSS)	0.233	0.112	1.03	0.146	0.458	0.394	0.765
tCOD	(mg L^{-1})	2443	7109	NA	4301	1905	3561	NA
cBOD	(mg L^{-1})	NA	NA	247	NA	NA	NA	143
TPS	(mg L^{-1})	797.2	1366	NA	636.0	160.3	664.4	NA
TN	(mg L^{-1})	NA	NA	23.8	NA	NA	NA	29.0
TKN	(mg L^{-1})	NA	NA	24.4	NA	NA	NA	27.2
DIN	(mg N per L)	15.3	12.6	NA	3.20	15.9	8.85	NA
Na^+	(mg Na per L)	51.1	79.4	NA	104.2	71.0	109.0	NA
NH_4^+	(mg N per L)	6.53	2.33	19.5	1.26	15.9	7.95	18.9
K^+	(mg K per L)	13.2	14.5	NA	17.4	12.6	16.9	NA
Ca^{2+}	(mg Ca per L)	13.6	14.0	NA	38.1	48.9	53.0	NA
Mg^{2+}	(mg Mg per L)	3.60	8.45	NA	29.4	9.94	15.0	NA
Cl^-	(mg Cl per L)	88.3	112.0	NA	150.0	93.2	137.0	NA
NO_2^-	(mg N per L)	1.27	0.468	NA	0.113	0.00	0.754	NA
NO_3^-	(mg N per L)	7.50	9.77	NA	1.83	0.067	0.145	NA
PO_4^{3-}	(mg PO_4 per L)	1.10	2.09	NA	3.11	3.77	2.97	NA
SO_4^{2-}	(mg SO_4 per L)	3.88	1.54	NA	13.6	7.80	12.7	NA

[a] a = Cultivations used for material strength analysis.

of the cultivation depending on the initial cultivation size and the number of vials used for destructive sampling during the cultivation. Table 2 summarizes the outcome of the cultivation sets, including the final number of vials remaining, how many of those vials formed granules, and the number of granules that formed either spheres or disks.

Among these seven cultivations, four sets were inoculated with activated sludge from the Amherst wastewater treatment plant (Amherst, MA), which operates at a solids retention time (SRT) of 10–15 days. The Amherst plant primarily receives municipal wastewater. The remaining three cultivations utilized activated sludge from the Hadley wastewater treatment plant, which employs a conventional activated sludge process with a 10 days SRT (Hadley, MA). The Hadley plant receives influent wastewater from residential, commercial, and agricultural sources. The measured initial water quality parameters and biomass characteristics of all cultivation sets are presented in Table 1. Each cultivation was named based on the source of the activated sludge and the percentage of vials in the cultivation that produced spheres. For example, "Am-100" indicates a cultivation using Amherst activated sludge that yielded only spheres, while "Ha-14.3" indicates a cultivation using Hadley activated sludge with 14.3% spheres, making it a disk-forming cultivation.

2.2. Characterization of photogranular morphology

For the remaining vials in each cultivation set, a shake test was conducted based on the procedure outlined by Stauch-White *et al.*[9] This involved three firm vertical agitations per vial, followed by visual inspection to ensure the aggregate maintained its form. Successful granulation was indicated if the granule remained intact with minimal or no particle clouds in the bulk liquid. The entire cultivation set was considered successful if at least 50% of the total vials were granulated. Through the shake test and visual assessment, OPGs were classified as either disks or spheres.

Table 2 Summary of the final morphology for the remaining vials at the end of each cultivation period[a]

Cultivation name	Sludge source	Total vials	Total OPGs formed	Spherical OPGs	Disk OPGs	Spherical OPG formation (%)	Cultivation morphology
Am-100	Amherst	20	20	20	0	100	Sphere
Ha-100	Hadley	13	13	13	0	100	Sphere
Am-68.9 a	Amherst	119	119	82	37	68.9	Sphere
Ha-27.8	Hadley	20	18	5	13	27.8	Disk
Am-17.1	Amherst	36	35	6	29	17.1	Disk
Ha-14.3	Hadley	36	35	5	30	14.3	Disk
Am-13.8 a	Amherst	110	80	11	69	13.8	Disk

[a] a = Cultivation results were used only for material strength analysis.

All aggregates exhibited an ellipsoidal shape in their final form, characterized by three perpendicular axes labeled as a, b, and c, corresponding to the radial length of the axes. By visual inspection, if an aggregate observed one semi-axis larger than the other two, it was considered a disk (Fig. 1). Otherwise, the aggregate's morphology was categorized as a sphere when all the semi-axes lengths were of equal length. Among the seven cultivation sets, three predominantly developed spherical photogranules in the remaining vials at the end of the cultivation period (Table 2). The cultivation set was labeled as either disk-forming or sphere-forming if 50% of the formed granules exhibited the same morphology. Spherical OPG formation was calculated as the ratio of the number of spherical OPGs to the total number of OPGs formed in each cultivation. Cultivations with 50% or more spherical OPG formation were classified as sphere-forming, while those with less than 50% were classified as disk-forming.

2.3. Mechanical properties measurement

To explore the mechanical properties of sphere and disk morphologies, the material strength of OPGs was assessed in two additional cultivations, Am-68.9 (sphere) and Am-13.8 (disk) using nano-compression testing. The compression results were used to determine the yield shear stress (τ_y), which is a measure of the maximum stress tolerated by the granule before permanent deformation occurs, and the stiffness of the granule (E), a measure of a granule's resistance to elastic deformation under stress, for each cultivation.

In the Am-13.8 cultivation, out of 110 vials, 30 failed to aggregate into granules. The remaining vials successfully formed aggregates, with 13.8% resulting in spheres and the rest forming disks. In contrast, the Am-68.9 cultivation formed 119 aggregates out of 119 total vials, with a significant proportion of these aggregates adopting a spherical morphology (68.9%). After the cultivation period, ten vials containing formed disks from the Am-13.8 cultivation and twelve vials containing spherical aggregates from the Am-68.9 cultivation were randomly selected. These samples underwent vertical compression to quantitatively assess their mechanical and elastic properties.

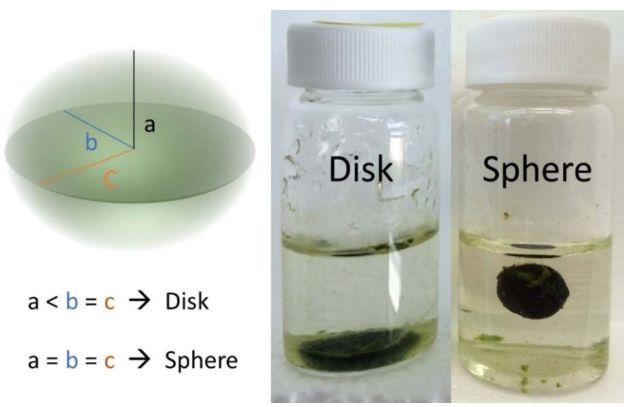

Fig. 1 Categorization of hydrostatic photogranules morphology based on semi-axes length. The left granule is an example of a disk, while the right granule is categorized as a sphere.

Each OPG was transferred onto a submerged flat aluminum substrate under sterile conditions and subjected to compression loading using a GeoJac loading frame (Trautwein Soil Testing Equipment Inc.) equipped with a miniature load cell (Load Cell Central; Model EGC-50) with dimensions of 50 × 50 × 50 mm. The load cell was placed inside the acrylic glass enclosure within the loading frame to prevent air and dust disturbances. The loading cell had a capacity of 50 g (490 mN) and a resolution of 0.02 nM. Quasi-static loading was applied to individual OPGs at a constant displacement rate of 0.05 mm min^{-1} with unloading cycles. An image of the loading frame and load cell are depicted in Fig. S1 in ESI.†

As the OPGs exhibited various shapes, a nominal diameter, D_o, was employed to normalize the size of OPGs.[22]

$$D_o = \frac{m_o}{\rho_o A_o} \quad (1)$$

where m_o is the mass of an OPG in grams, ρ_o is the average density of OPGs, measured as 1.15 mg cm^{-3}, and A_o is the nominal cross-sectional area of the granule.

The average diameter of a single OPG was calculated by averaging the lengths of the maximum, diagonal, and minimum radial lengths of the OPGs. Two-dimensional images of the OPGs were taken using a digital camera on the loading system to estimate the cross-sectional area and assumed a circular shape. To maintain consistency across measurements, a Vernier caliper with a precision of 0.02 mm was first used to measure the maximum, diagonal, and minimum lengths of the bottom surface of the OPGs. The average length of the bottom surface for each sample was then calculated from these measurements. Assuming the bottom surface is circular, this average length was used as the diameter to calculate the cross-sectional area of the sample. The Hertz elastic contact theory was applied to analyze the load-deformation curves, and the reduced modulus (E_r) is reported as a measure of the contact stiffness between an OPG and the glass plate.[23]

$$E_r = \frac{3P}{\left(D_o d^3\right)^{1/2}} \quad (2)$$

where P is the load applied to the tested OPG and d is the sum of deformation between two OPG hemispheres.

To identify the elastic stage beyond which the tested OPG started yielding, the Hertzian elastic contact line was determined by plotting $3P/{D_0}^{1/2}$ *versus* $d^{3/2}$ (as given in eqn (2)). The start of plastic yielding is marked by locating the point where the Hertz elastic contact line deviates from the experimental load-deformation curve. The yield shear stress, τ_y, of the OPG is then computed as:

$$\tau_y = 0.31 p_{max} = 0.31\left(\frac{24 P_y {E_r}^2}{\pi^3 D^2}\right)^{1/3} \quad (3)$$

where p_{max} is the maximum pressure within the contact area at the start of plastic yield and $P_y$is the applied load when yielding occurs.[24] Finally, the elastic modulus, which is a measure of the material's stiffness, was also calculated using the following formula.

$$E = E_r(1 - v^2) \quad (4)$$

where E is the elastic modulus of the OPG, and v is its corresponding Poisson's ratio. This study assumed a Poisson ratio of 0.3, typical for general granular material.[24]

Linearized two-parameter Weibull probability distributions (WPD) were employed to predict failure behavior regarding the mechanical properties of the OPGs in each cultivation. The Weibull cumulative distribution function was employed to model both E and τ_y of each tested OPG, described by the following equation.[25]

$$F(x, \lambda, k) = 1 - e^{-\left(\frac{x}{\lambda}\right)^k} \quad (5)$$

$$\ln(-\ln(1 - F(x))) = k \ln\left(\frac{x}{\lambda}\right) \quad (6)$$

where x is the random variable of interest, k is the shape parameter or the Weibull Modulus, and λ is the scale parameter, or nominal stress, of the distribution. The Weibull modulus (k) serves as an indicator of structural variability, with values exceeding one suggesting more uniform behavior due to evenly distributed flaws, leading to higher strength and less scattered properties. The scale parameter, λ, represents the characteristic strength at which 63.2% of the material will have failed. Eqn (6) illustrates the regression line between $\ln(-\ln(1 - F(x)))$ and $\ln(x_i)$, but the corresponding Fi for each independent variable x_i is yet to be determined. To address this, the mean rank method, which considers the relationship between the rank of experimental data point i and the total number of all data points n, is employed using the following equation:[26]

$$F_i = \frac{i}{n+1} \quad (7)$$

Using eqn (7), the experimental data points can be fitted with eqn (6) to obtain k and b values through linear regression. These values then aid in determining the shape parameter λ with the following equation:

$$\lambda = e^{-\frac{b}{k}} \quad (8)$$

Finally, the statistical mean value or characteristic value of extracted mechanical properties is determined using the gamma function:

$$E(x) = \lambda \Gamma\left(1 + \frac{1}{k}\right) \quad (9)$$

2.4. Chemical analysis

Chlorophyll content, total and volatile suspended solids, and total chemical oxygen demand (tCOD) were measured following the APHA standard methods.[27] Soluble COD (sCOD) reported here is the COD of the liquid fraction of the sample filtered through a 0.45 μm filter, and total COD (tCOD) is the COD of the sample unfiltered and includes the biomass fraction. Dissolved organic carbon (DOC) and dissolved total nitrogen (DTN) were measured using a Shimadzu TN/DOC analyzer (Shimadzu TOC-VCPH). Additionally, nitrate, nitrite, ammonium, phosphate, sulfate, sodium, potassium, calcium, and magnesium were measured using a Metrohm 850 Professional Ion Chromatograph. Dissolved inorganic nitrogen (DIN) was calculated as the sum of ammonia, nitrate, and nitrite. Total polysaccharides (TPS) were measured by homogenizing samples and utilizing the DuBois method.[28] All samples analyzed were measured in triplicate for each parameter, and the average results are presented.

Extracellular polymeric substances (EPS) were extracted using the alkaline extraction method.[29] Three randomly selected vials, each containing 10 mL, were destructively sampled. Subsequently, each individual vial was transferred to a sterile 50 mL centrifuge tube and centrifuged at 12 000 rpm (20 850 g) for 20 min at 4 °C. The supernatant, obtained after centrifugation, was collected and filtered through 0.45 μm cellulose filters to analyze the chemical composition of the soluble EPS fraction. Meanwhile, the remaining pellets were resuspended in 20 mL of phosphate buffer solution (10 mM NaCl, 1.2 mM KH_2PO_4, and 6 mM Na_2HPO_4).[29] The buffer's conductivity was adjusted to replicate the conductivity of the activated sludge inoculum at a pH of 7.2.[30] Each replicate underwent homogenization for 30 seconds. The pH of the homogenized samples was adjusted to pH 11 using 1 M NaOH and mixed on a shaker table at 400 rpm for 2 hours in the dark at 4 °C.[30] A vial with only phosphate buffer adjusted to pH 11 with NaOH served as a blank control. Following extraction, each sample was centrifuged at 4 °C at 12 000 rpm (20 850 g) for 20 minutes. The supernatant was stored at −20 °C in aliquots until chemical analyses were conducted. Proteins (PN) and humic acids (HA) were measured using the modified Lowry method, and polysaccharides (PS) were measured as previously mentioned.[29,31,32] Standards such as bovine albumin serum, humic acids, and glucose were employed for proteins, humic acids, and polysaccharides, respectively.

2.5. Correlation and principal component analysis (PCA)

Prior to PCA, seventeen initial water quality parameters from each cultivation were first correlated with their corresponding final spherical morphology percentages to identify potential dependencies influencing morphology outcomes. While the Pearson correlation is the most-widely used tool, it assumes that both variables follow normal distributions and are linearly correlated. To test the assumptions, all variables underwent normality testing using the Shapiro–Wilkes test with $\alpha = 0.05$ to determine which correlation method best suited the data. Since sphere formation, Chl a, and Chl c did not exhibit normal distributions, a non-parametric analysis using Spearman's rank correlation was conducted for the various combinations of variables to measure the degree of association. Associations between two variables were considered strong if the correlation coefficient was equal to or greater than 0.60.

Principal component analysis (PCA) was performed on five out of the seven cultivations presented in this study to determine patterns in the data. For the PCA, the eigenvalues and proportion of variance for each principal component were determined using all 17 variables. The quality of variable

representation was evaluated by calculating the square cosine values. The correlation analysis and PCA were all constructed using *R*.[33]

3. Results and discussion

3.1. The interplay between OPG morphology, cyanobacterial growth, and EPS production

The five hydrostatic cultivations, conducted under uniform light conditions, successfully matured OPGs after 28 days of incubation. The initial (day 0) chlorophyll concentrations and sludge concentrations are presented in Table 1. The unique initial profiles of each activated sludge suggest a diverse microbial community, including a mix of algae, cyanobacteria, and other phototrophic microorganisms, each contributing differently to the chlorophyll composition. In all five cultivations, the Chl *a* and Chl *b* concentrations experienced a rapid increase during the first two weeks of cultivation, indicating the phototrophic bloom period (Fig. 2a and b). The 5-fold increase in the chlorophyll *a*/*b* ratio over the same period implies cyanobacterial enrichment, considering chlorophyll *a* is present in both cyanobacteria and green algae, while chlorophyll *b* is absent in cyanobacteria (Fig. 2d). This observation aligns with microscopic findings, where green algae typically initiated the bloom.[1,3,4] However, filamentous cyanobacteria emerged as the dominant phototrophic group for the remainder of the cultivation period.[1,3,4] This assertion is substantiated by previous studies that utilized molecular tools, confirming the enrichment of cyanobacteria within hydrostatic photogranules.[1,9]

Mature photogranules from spherical cultivations, mainly Am-100 and Ha-100, exhibited lower Chl *a* concentration (5.97 ± 0.10 and 7.40 ± 0.38 mg L^{-1}, respectively), compared to photogranules from disk cultivations with Chl *a* concentration ranging between 8.13–11.7 mg L^{-1}. This suggests a higher phototrophic content in disk-shaped photogranules compared to spherical ones. The observed trend aligns with the notion that disk-shaped photogranules, with their slimmer thickness of approximately 3 mm, could potentially improve nutrient diffusion and light penetration, thereby enhancing the growth of phototrophic organisms. Based on the literature, the phototrophic outer layer developed in all statically formed photogranules is consistently around 500–1000 μm thick.[1] Considering both sides of the disk granules, phototrophs can occupy approximately two-thirds of the entire thickness of the disk granules. Conversely, spherical photogranules, with a larger thickness ranging from 10 to 20 mm, might face challenges related to light and nutrient availability in the inner biomass layers. This situation could potentially restrict the growth of phototrophic organisms deeper within the granules. Based on the reported depth of the phototrophic layer in the literature, phototrophs in spherical granules can occupy only 10−20% of the entire granule thickness, which is significantly less compared to disk-shaped granules.[1] This phenomenon aligns with established principles in microbial ecology, where structural attributes of granules play a pivotal role in modulating the microenvironment and subsequently influencing microbial community dynamics.[34–36] The higher Chl *a*/*b* ratio in disk-shaped photogranules than in spherical ones suggests that

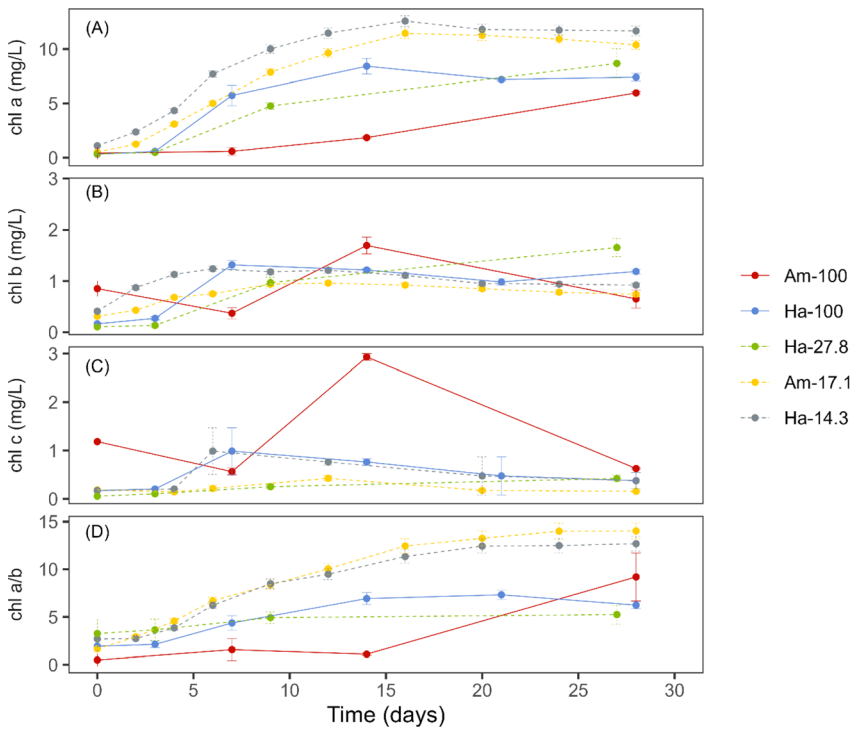

Fig. 2 Chlorophyll concentration during hydrostatic photogranulation. (A)Chlorophyll *a*, (B) chlorophyll *b*, (C) chlorophyll *c*, and (D) the ratio of chlorophyll *a*/*b*. The solid lines represent data from cultivations dominated by spherical granules, while the dashed lines represent data from cultivations dominated by disk-shaped granules.

the increase in phototrophic content was likely due to the higher cyanobacterial content in the disk-shaped photogranules.

EPS, a complex mixture of biopolymers secreted by cyanobacteria and other microbes, are known to enhance the cohesion and adhesion of cells, facilitating the formation and stability of photogranules.[4] Fig. 3 presents the concentrations of biomass-bound EPS during the granulation period for three cultivations: Ha-100 (sphere), Am-17.1 (disk), and Ha-14.3 (disk). Both EPS PN and HA exhibited decreasing trends over the initial 10–15 days of cultivation, followed by stabilization for both spherical and disk-like cultivations (Fig. 3a and c). The decreasing trend of EPS PN is common in hydrostatic granulation, as cyanobacteria have been reported to utilize EPS as a carbon source for their growth within photogranules.[37] This ability gives cyanobacteria an advantage over other phototrophs, contributing to their dominance in the OPG biomass. EPS PS showed a minor increase for both spherical and disk-like cultivations and then stabilized or slightly decreased until the end of the cultivation period (Fig. 3b). The stability of EPS PS in spherical OPG cultivations aligns with findings from previous studies investigating hydrostatic photogranulation.[3,4] In contrast, the PN/PS ratio decreased during the first 7 days of hydrostatic granulation and then stabilized (Fig. 3d).

Compared to disk-shaped photogranules, spherical photogranules exhibited significantly lower concentrations of both EPS PN and EPS PS, suggesting improved granulation under the limitation of EPS. This finding aligns with previous hydrostatic photogranules studies, indicating that cyanobacteria granulate more effectively under the limitation of both EPS and Fe bound with EPS.[3,12,38] Conversely, the PN/PS ratio of spherical photogranules was much higher than that of disk photogranules. The PN/PS ratio, indicating the proportion of hydrophobic to hydrophilic polymers in EPS, can offer insights into the settleability of granules. Hydrophilic constituents tend to exhibit enhanced settling capabilities by effectively integrating within the aqueous phase.[39,40] Similar EPS transformation trends have also been reported in aerobic sludge granules, where granules exhibit higher PN concentrations than PS, resulting in PN/PS ratios of 1.4–1.6.[41] EPS PN are found within the core of aerobic granules, contributing to increased granular stability due to enhanced internal hydrophobicity.[41,42] In contrast, flocs have higher concentrations of PS, with PN/PS ratios closer to 0.5.[41] Interestingly, the growth mechanism of small aerobic granules, similar to observations about OPGs, has been hypothesized to involve self-propagation rather than self-aggregation.[1,3,4,43] In aerobic granules, this phenomenon is attributed to their reduced PN/PS ratios, leading to diminished hydrophobicity, a factor aiding granules in compacting during the granulation process.[44]

3.2. The role of divalent cations in hydrostatic photogranulation

The presence of metal cations in wastewater plays a significant role in bridging negatively charged surface sites, aiding in the formation of cell aggregates.[45–47] With further maturation, these

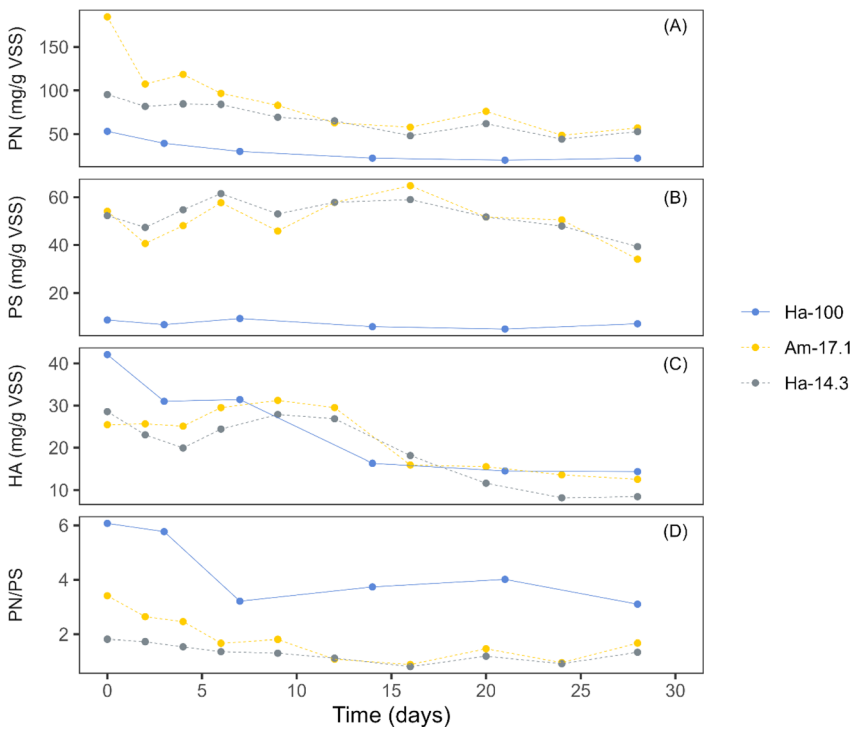

Fig. 3 Changes in extracellular polymeric substances (EPS) concentrations during the granulation process. (A) Biomass-bound EPS proteins (PN), (B) biomass-bound EPS polysaccharides (PS), (C) humic acids (HA), and (D) PN/PS ratio. Data for the Ha-100 cultivation are reproduced from Kuo-Dahab *et al.* (2018).[4] The solid line represents data from cultivations dominated by spherical granules, while the dashed lines represent data from cultivations dominated by disk-shaped granules.

aggregates develop into robust granular structures. Divalent cations, especially those with increasing ionic sizes, exhibit a higher binding affinity to EPS, while monovalent cations can displace divalent cations, weakening the aggregate structure.[45–47] Fig. S2† illustrates the soluble concentrations of Na^+, K^+, Ca^{2+}, Mg^{2+}, and the monovalent to divalent cations (M/D) ratio for the five cultivations. Although there are no significant patterns in the concentrations of Na^+ and K^+ among cultivations with different morphologies, there is a noticeable distinction in the initial availability of cations, especially Ca^{2+} and Mg^{2+}, between disk and sphere cultivations. In the early stages of the photogranulation period for cultivations that predominantly produced disks (*i.e.*, Ha-27.8, Am 17.1, Ha-14.3), there was a higher initial concentration of both Ca^{2+} and Mg^{2+}. Notably, three of the four disk cultivations exhibited a clear peak in Ca^{2+} and Mg^{2+} concentrations around days 3–4. During this period, the activated sludge underwent a settling process and experienced a certain degree of decay, potentially leading to the release of cations into the bulk liquid before initiating phototrophic growth. This increase in cation concentrations during the photogranulation process was not observed in spherical cultivations. The M/D ratio for three disk cultivations all exhibited a significant decrease in the ratio between time 0 and 3–6 days, with some reaching values as low as 0.37 before the uptake of Ca^{2+} and Mg^{2+} began during the photogranulation and EPS production stages. From a reactor operation perspective, the M/D ratio also provides insights into the dewatering and settling characteristics of the photogranules. Values of M/D greater than two have been associated with a deterioration in both of these characteristics.[48] The spherical OPG cultivations exhibited final M/D ratios ranging from 2.5 to 2.7, while the disk cultivations resulted in M/D values ranging from 1.6 to 2.1. Recent observations of hydrostatically grown OPGs indicated higher density and settling velocity compared to hydrodynamically grown OPGs, although the morphology of the hydrostatic granules was not characterized.[11] Nevertheless, the findings from this study suggest that hydrostatically grown disk-shaped granules may possess improved settleability compared to spherical granules.

3.3. Inorganic nitrogen profile

In all cultivations, the initial concentrations of dissolved inorganic nitrogen (DIN) in the bulk liquid ranged from 3 mg N per L to 15.9 mg N per L (Fig. 4). Notably, the initial DIN concentrations primarily comprised both ammonia and nitrate, with minimal levels of nitrite being detected. During the initial week of incubation, all photogranulation cultivations demonstrated substantial decreases in DIN concentrations, concomitant with reductions in the concentrations of NH_4^+ and NO_3^- (Fig. 4). Additionally, a slight decrease in nitrite levels was also observed. After the first week, the concentrations of all nitrogen species stabilized. The observed decreases in nitrogen species were likely attributed to phototrophic utilization within cultivation vials, whether this cultivation resulted in spherical or disk-shaped photogranules.

It is crucial to note that in the two cultivation sets Am-100 and Ha-100, which led to the development of spherical granules, observed decreases in the concentrations of DIN, NH_4^+,

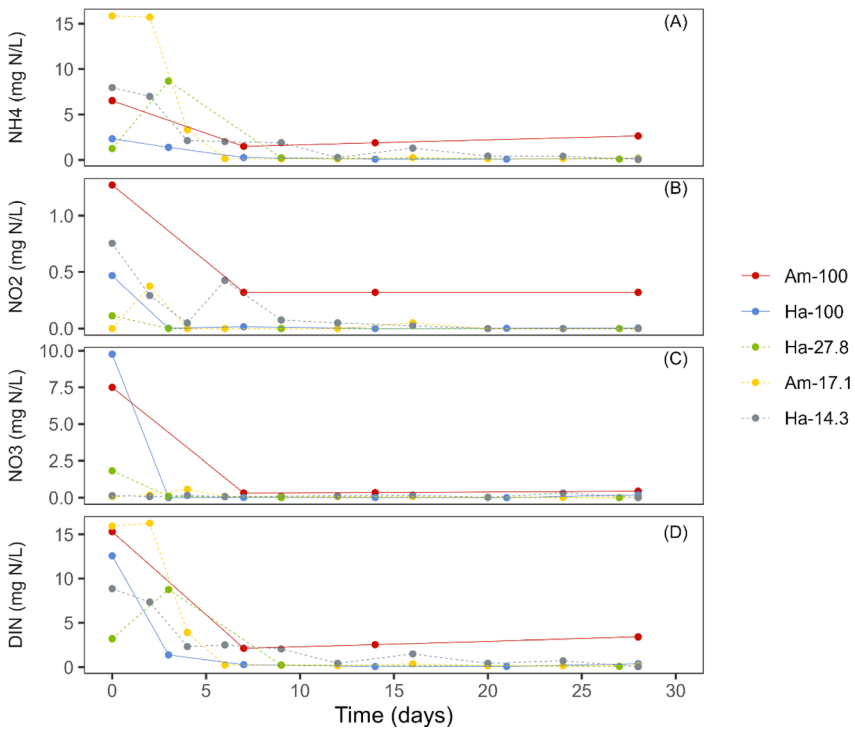

Fig. 4 Concentrations of nitrogen species during the granulation process. (A) NH_4^+, (B) NO_2^-, (C) NO_3^-, and (D) DIN. The solid lines represent data from cultivations dominated by spherical granules, while the dashed lines represent data from cultivations dominated by disk-shaped granules.

and NO_3^- during the initial week were sharp (Fig. 4). In contrast, the cultivation sets resulted in the formation of disk-shaped granules demonstrated increases or stability in both DIN and NH_4^+ within the initial days of operation, followed by rapid decreases. The observed elevation in NH_4^+ concentrations in these cultivation sets was likely attributed to biomass decay. Similar patterns for ammonium consumption have been observed for other hydrostatic granulation studies.[3,9]

It is also noteworthy that the three cultivations that showed initial DIN concentrations of less than 10 mg L^{-1} formed disk-shaped photogranules (Fig. 4). This finding aligns with Stauch-White *et al.*,[9] who noted that cultivations with DIN concentrations below 9 mg L^{-1} did not yield spherical mature granules by the end of the granulation process.

In terms of nitrogen species, it appears that both ammonia and nitrate play essential roles in hydrostatic photogranulation. Ammonium is generally favored as a nitrogen source by most green algae and cyanobacteria compared to nitrate.[49] This preference may explain the higher chlorophyll a concentrations observed in disk cultivations, where ammonia constitutes a significant fraction of the DIN, promoting rapid phototrophic proliferation. Nitrate (NO_3^-) might have been removed through biomass assimilation or denitrification (conversion of NO_3^- to N_2). In aerobic granular sludge, denitrification was found to accelerate granule formation through two pathways: (1) the production of nitric oxide (NO) as an intermediate, known to induce cell aggregation and biofilm formation in bacterial cultures, and (2) generating alkalinity and creating conditions favorable for carbonate precipitation, which could provide nuclei for granulation and contribute to making the granules denser.[50,51]

3.4. Predictors of mature OPG morphology

The temporal data from the five cultivations showed that several water quality parameters and biomass characteristics influence the formation of a distinct granule morphology. The relationships between measured initial parameters and final morphology were statistically analyzed for 17 variables using Spearman's rank correlation analysis. Furthermore, PCA analysis was also conducted to to reduce the dimensionality of the data set and identify which group of variables most strongly correlated to a particular morphology.

First, we utilized a Spearman's correlation matrix to analyze the interactions among 17 selected parameters and their influence on OPG morphology, as shown in Fig. 5. It was found that phototrophic growth within photogranules, indicated by

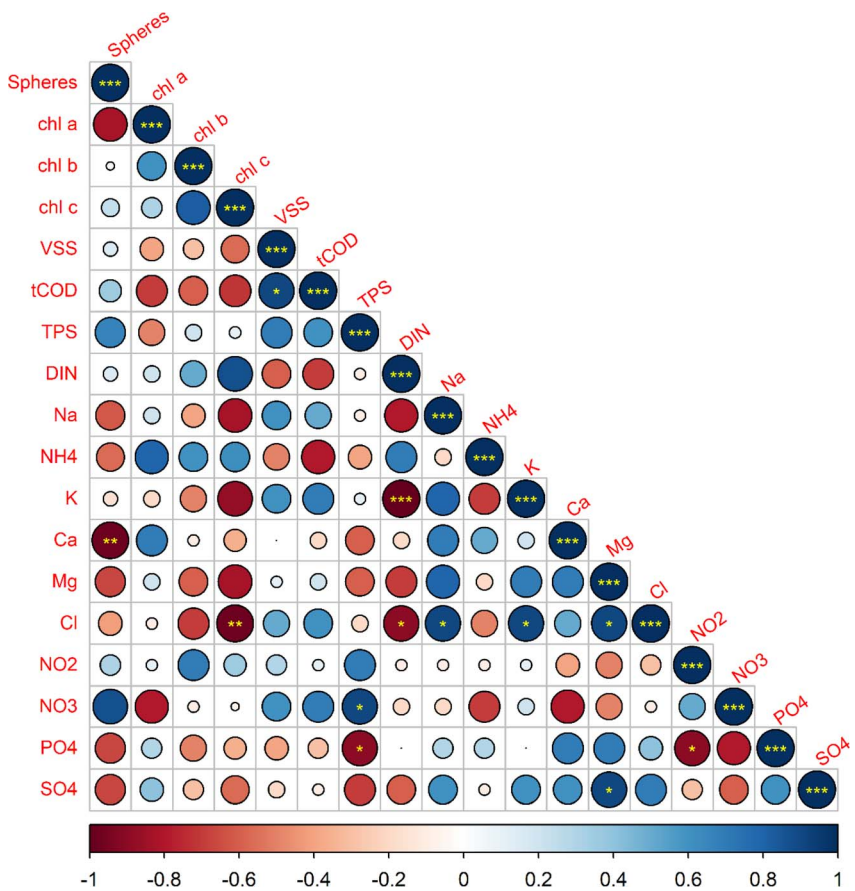

Fig. 5 Correlation matrix of Spearman's rank correlation coefficients between 18 parameters including 17 initial water quality measurements and the final cultivation set morphology. Blue represents a positive correlation and red represents a negative correlation. The circle size is proportional to the absolute value of the correlation coefficient. The stars represent the significance level where *p*-values 0.05 = *, 0.01 = **, and 0.001 = ***.

chlorophyll *a*, *b*, and *c* concentrations, exhibited positive correlations with both the initial DIN and ammonia concentrations in the cultivation vials. Among chlorophyll types, Chl *a* exhibited a strong positive correlation with NH_4^+ and a strong negative correlation with nitrate. This suggests that the abundance of phototrophs containing chlorophyll *a* but not *b* or *c*, such as cyanobacteria, are negatively correlated with initial nitrate concentrations. Diatoms and dinoflagellates, indicated by Chl *c*, demonstrated a strong positive correlation with DIN and a strong negative correlations with chloride (Cl^-), magnesium (Mg^{2+}), phosphate (PO_4^{-3}), potassium (K^+), sulfate (SO_4^{2-}), and sodium (Na^+). Chl *a* also shows a strong negative correlation with sphere formation in comparison to Chl *b* and Chl *c*, which suggests that an initial lower abundance of phototrophs with chlorophyll *a* are linked to the formation of spherical OPGs.

On the other hand, OPG sphericity exhibited strong positive correlations ($r > 0.6$) with both the initial nitrate concentration in the soluble fraction and the total polysaccharide (TPS) concentration within biomass. This suggests that higher initial concentrations of nitrate and TPS are associated with a greater likelihood of preferential development of spherical OPGs. On contrary, OPG sphericity exhibited strong negative correlations with ammonium (NH_4^+), sodium, calcium (Ca^{2+}), magnesium, phosphate (PO_4^{-3}) and sulfate (SO_4^{2-}). Notably, sphere-forming cultivations AM-100 and Ha-100 commenced with initial PO_4^{-3} concentrations below 2.1 mg P/L, while all disk cultivations had initial concentrations ranging between 3.0 mg P/L and 4.6 mg P/L.

The PCAbiplot, as depicted in Fig. 6, revealed distinct clusters based on the final morphology of OPGs. PCA effectively segregated two sphere cultivations in the upper left quadrants and the three disk cultivations in the lower right quadrants. The PCA biplot suggests a stronger correlation between the development of spherical OPGs with TPS and NH_4^+ *versus* Chl *a*, Chl *b*, and Chl *c*. This suggests that the initial activated sludge characteristics, like EPS, may play an important role in the formation of spherical *versus* disk formation, as a large percentage of activated sludge biomass can be attributed to EPS or polysaccharides and proteins. The primary contributor to principal component 1 was Na^+(11.0%), followed by SO_4^{2-}(10.3%), Cl^- (9.9%), Mg^{2+} (9.8%), DIN (8.6%) and K^+ (8.3%) (Fig. S3†). Principal component 2 was influenced by TPS (16.4%), NH_4^+ (16.3%), tCOD (14.6%), VSS (12.4%), NO_3^- (9.5%), and PO_4^{3-} (6.3%) (Fig. S4†). PC1 primarily measured inorganic ions found in activated sludge while PC2 measured biomass parameters and nutrients. PC1 accounts for 48.4% of proportion of variance, while PC2 accounts for 31.4%. The combined variance accounted for by both PC's is 79.8%. Out of these variables, 10 are considered water quality parameters (Cl^-, K^+, NO_3^-, Na^+, NH_4^+, Ca^{2+}, Mg^{2+}, PO_4^{3-}, SO_4^{2-}, and DIN), while the remaining TPS, tCOD, and VSS are considered sludge biomass characteristics. The cultivation Am-100 (Sphere) lies on

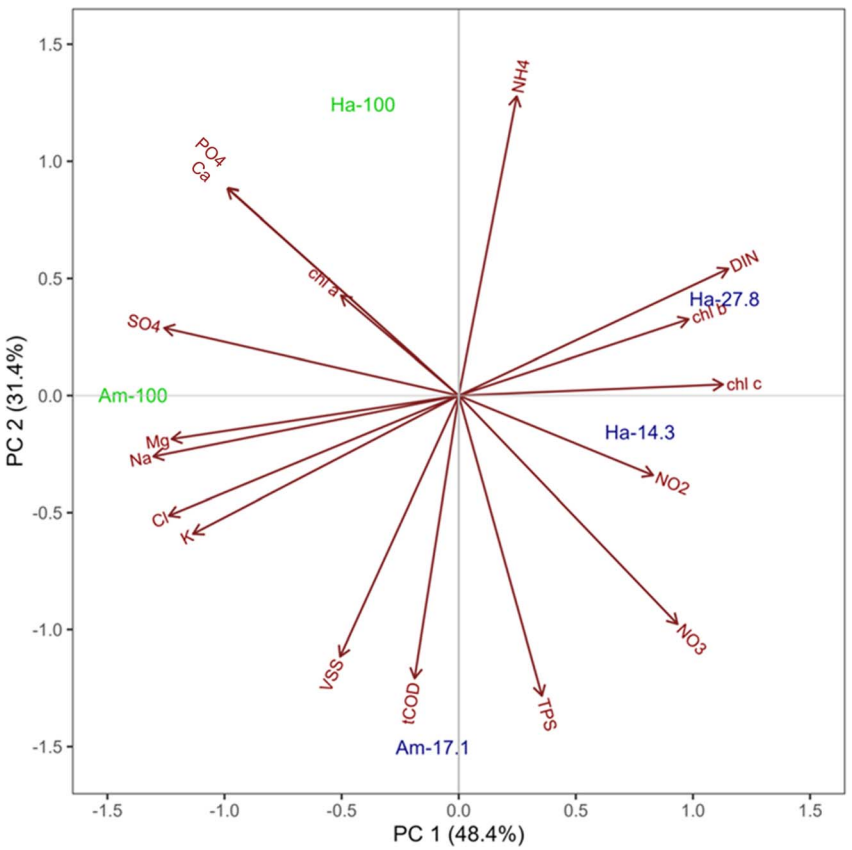

Fig. 6 Principal component analysis biplot depicting all 17 initial water quality variables from five OPG cultivations, with majority spheres represented in green and majority disks in blue.

the PC1 axis which suggests it has a strong positive correlated with the initial inorganic ions. Cultivation Am-17.1 (disk) lies on the PC2 axis which suggest it has a strong positive correlation with initial biomass composition (TPS, tCOD, and VSS) and nutrients (NH_4^+, NO_3^-, and PO_4^{3-}). This observations further suggests that while a multitude of factors may influence the formation of a specific granule morphology, the initial availability of nutrients can impact the rapid growth of cyanobacteria and lead to disk-shaped granules. The PCA highlights the importance of these specific water quality parameters and activated sludge characteristics in influencing photogranulation processes. Additionally, these factors could serve as valuable indicators of successful or unsuccessful photogranulation.

3.5. Variability of temperature and light

The initial surface temperatures and light intensities applied to each scintillation vial were recorded for the cultivation sets Am-13.8 and Am-68.9, along with the final morphology of each OPG in the vials. The formation of spherical OPGs was more prevalent in cultivations with higher localized temperatures despite both cultivations being exposed to similar light intensities (8.28 ± 1.32 kLux for Am-13.8 and 8.25 ± 1.66 kLux for Am-68.9) (Fig. 7a and b). The temperature density curve for all spherical OPGs in both cultivations exhibited a positively skewed bimodal distribution (Fig. 7c). The formation of spherical structures increases with temperatures beyond 21.5 °C, with approximately 41.9% of spherical photogranules exhibiting localized temperatures between 23 to 23.5 °C.

The distribution of light intensity for disk-shaped OPGs displayed a bimodal pattern, with each peak corresponding to a specific cultivation set, indicating similar densities. It is important to highlight that an increase in environmental temperature from 20 °C to 25 °C may lead to an increase in cyanobacterial growth.[52] This is consistent with the optimal growth conditions for cyanobacterial species, which are often associated with higher temperatures (≥25 °C).[53,54] While there seems to be a strong correlation between high localized temperatures and sphere formation, the growth of cyanobacteria is influenced by various factors, including the availability of inorganic nitrogen and phosphorus species, metal cations, COD, and photosynthetic activity, all of which play influential roles in determining the final morphology of OPGs.

3.6. The mechanical properties of OPGs depend on mature morphology

Understanding the distinct mechanical properties of various OPG morphological types is crucial, considering the consistent prevalence of a specific morphology across diverse hydrostatic cultivations. The practical implications of how these different shapes behave in wastewater treatment reactors further underscore the significance of this investigation. The chosen hydrostatic photogranules attained a final average nominal diameter (D_o) of 6.65 ± 1.67 mm for Am-13.8 (disk) and 7.96 ± 1.90 mm for Am-68.9 (sphere). Notably, there was a strong positive linear correlation between the yield shear stress (τ_y), our the maximum stress tolerated by the granule before

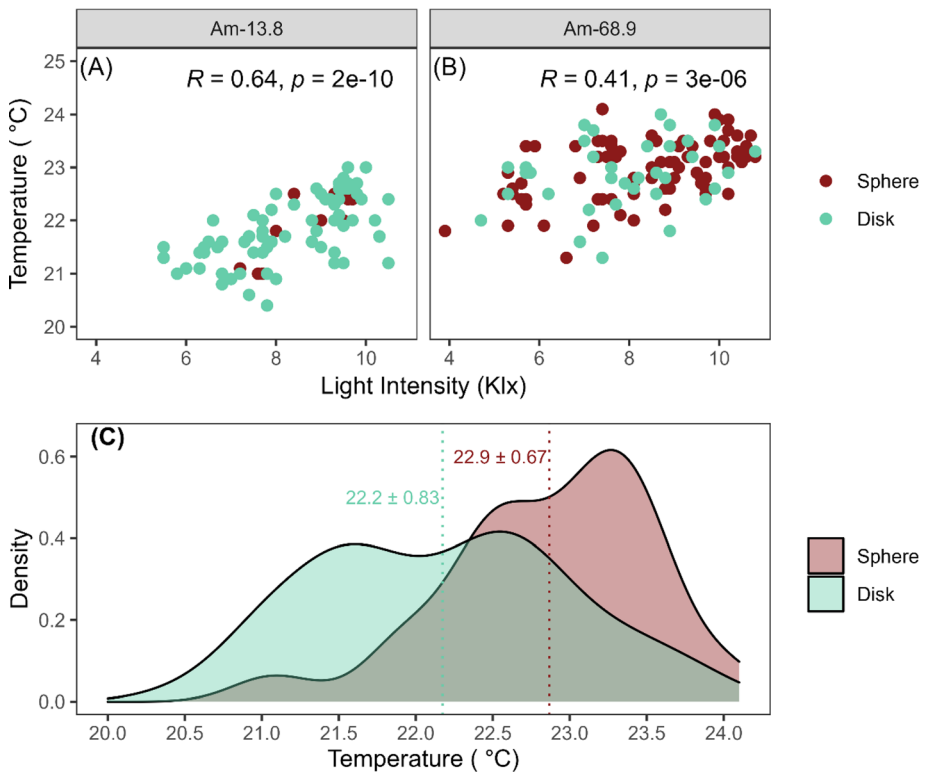

Fig. 7 Light intensity and temperature of cultivation vials. (A) Temperature in cultivation Am-13.8, and (B) temperature in cultivation Ha-68.9, and (C) the combined density distribution and mean temperatures observed for either disks or spheres regardless of cultivation set.

permanent deformation occurs, and the stiffness of the granule (E), a measure of how elastically or plastically the granule behaves, regardless of the photogranule morphology (Fig. S5†). In Am-13.8, granules exceeding 6 mm in nominal diameter showed significantly lower E and τ_y values than smaller granules in the same set. Specifically, larger disk granules exhibited E values below 14 kPa and τ_y values below 0.4 kPa. The highest observed yield shear stress (τ_y) in Am-13.8 was 2.04 kPa, observed in a disk-shaped photogranule with a diameter of 5.87 mm. Noteworthy negative correlations were identified between the diameter of disk-shaped photogranules and both E and τ_y, indicated by non-parametric Spearman's rank correlation coefficients ($\rho = -0.59$ and $\rho = -0.55$, respectively). Conversely, the diameter of Am-68.9 spherical granules also displayed a negative correlation between the observed τ_y ($\rho = -0.27$) and E ($\rho = -0.22$); however, these results did not reach statistical significance.

The Weibull modulus estimates for both E and τ_y are presented in Table 3. Fig. S5† shows the Weibull distribution of the extracted mechanical properties (E, τ_y) for the two cultivations. All four cumulative WPD curves fit the supplied data linearly, with R^2 values higher than the critical point R^2 of 0.854 and 0.866 for Am-13.8 and Am-68.9 cultivations, respectively, which relates to a 95% confidence interval for small sample sets.

All Weibull modulus values were close to or slightly greater than 1, indicating a constant rate of failure concerning either E or τ_y. This suggests that flaws within photogranule structure result from random failure, irrespective of the morphologies developed in different cultivations. In terms of τ_y, disk-like exhibited higher values than spherical photogranules (0.605 kPa *vs.* 0.452 kPa). This suggests that disk-like photogranules may exhibit greater resistance to deformation from shearing compared to spherical granules. This resistance could be attributed to the higher abundance of filamentous cyanobacteria in disk-like photogranules. Filamentous cyanobacteria are known for their high shear resistance due to the substantial thickness of their cell wall, reaching up to 500 nm.[55–57]

Additionally, disk-like (*i.e.*, Am-13.8 cultivation) exhibited higher E values than spherical photogranules (*i.e.*, Am-68.9 cultivation), 21.06 kPa compared to 13.24 kPa, indicating greater stiffness and greater capacity to withstand elevated stress levels before undergoing plastic deformation. The observed E values fall within the range observed in other biofilms, such as *Pseudomonas aeruginosa* grown on solid substrates, which demonstrated E values closer to 5–60 kPa.[58] The higher stiffness of disk-dominated photogranules compared to spherical granules could be attributed to the increased EPS content within disk-dominated photogranules. In aerobic granular sludge, EPS are widely recognized as crucial contributors to microbial aggregation and play a key role in enhancing the compactness and mechanical stability of granules.[1,59]

The increased stiffness of disk-dominated photogranules can also be attributed to the higher initial concentrations of calcium (Ca^{2+}) and magnesium (Mg^{2+}) observed in their cultivation environment. This aligns with existing literature, which suggests that the stiffness of biofilms and cell aggregation is positively influenced by the availability of calcium and magnesium.[47,58] Calcium and magnesium ions are known to crosslink alginate, which is a significant component of the extracellular polymeric substances produced by microbes in biofilms.[47,60] Notably, alginate hydrogels, considered a reference material for investigating the mechanical properties of EPS, formed with Ca^{2+} cations, exhibited an E value of approximately 30 kPa, a similarity observed in OPGs from the Am-13.8 and Am-68.9 cultivations.[47] Additionally, studies by Lin *et al.*[61] demonstrated that the stiffness of aerobic granules increased with the number of crosslinks between alginate-like EPS and Ca^{2+} ions, resulting in a more robust gel structure than flocs. These findings suggest that hydrostatic OPGs form intricate networks of crosslinked biopolymers, facilitated by alkaline earth metals such as Mg and Ca. This process contributes to creating a stronger and stiffer material structure, with disk OPGs exhibiting notably higher strength and stiffness than their spherical counterparts.

Table 3 Statistical parameters (κ, λ, τ_y, E) parameters obtained from the linearized cumulative Weibull probability distributions

		Am-13.8 (disks)	Am-68.9 (spheres)
Yield shear stress, τ_y	κ	1.054	1.219
	λ (kPa)	0.605	0.452
	R^2	0.9557	0.8701
Elastic modulus, E	κ	1.272	1.127
	λ (kPa)	21.06	13.24
	R^2	0.8922	0.9546

3.7. Implications for wastewater treatment

The current study reveals a strong correlation between the morphology of hydrostatic granules and their mechanical strength. Disk-like hydrostatic photogranules demonstrated higher strength, stiffness, and greater resistance to deformation from shearing compared to spherical granules. This fundamental strength of disk-like hydrostatic photogranules translates into a more robust response to hydrodynamic shear within treatment reactors. Consequently, reactors seeded with disk-shaped granules will likely withstand turbulent conditions and maintain structural integrity during reactor operation. On the other hand, spherical photogranules, while exhibiting lower mechanical strength compared to their disk-like counterparts, offer distinct advantages in terms of rapid proto-granule production and disintegration efficiency under hydrodynamic shear. This makes them particularly advantageous during the critical startup phase of wastewater treatment reactors, where quick establishment and efficient granulation are paramount. The practical implications of these findings are significant for reactor operation and performance optimization. Tailoring the morphology of seed photogranules based on the desired operational outcomes can lead to tangible benefits. For instance, using disk-shaped granules can enhance resilience to shear forces, promoting stable reactor operation over extended periods. Conversely, utilizing spherical granules during the

startup phase accelerates granulation processes, expediting reactor readiness and improving overall efficiency. Strategies aimed at influencing granule morphology, such as nutrient supplementation and manipulation of hydrodynamic conditions during seeding, emerge as actionable approaches to optimize reactor performance. By understanding and leveraging the relationship between granule morphology and mechanical strength, wastewater treatment facilities can adopt targeted strategies for specific operational goals, ultimately enhancing overall efficiency and performance.

4. Conclusions

The study elucidates the intricate relationships governing the morphology and, thus, mechanical properties of oxygenic photogranules (OPGs) produced under hydrostatic conditions. Analysis reveals that environmental factors such as nutrient availability, light exposure, and the presence of divalent cations significantly influence granule morphology. Spherical granules are favored under elevated dissolved inorganic nitrogen (DIN) concentrations, while disk-dominated photogranules are strongly correlated with divalent cations concentrations. Temperature and light intensity also impact granule morphology, with higher localized temperatures correlating with spherical granule formation. Furthermore, the mechanical properties of granules, including their stiffness and resistance to shear stress, are influenced by morphological characteristics, with disk-shaped granules demonstrating higher stiffness attributed to elevated EPS content and crosslinking by divalent cations. These findings underscore the complexity between environmental factors, microbial dynamics, and granule morphology in hydrostatic OPG cultivation, offering valuable insights for optimizing wastewater treatment strategies and designing tailored approaches to enhance reactor performance and efficiency.

Author contributions

CJC: conceptualization, data curation, formal analysis, methodology, validation, visualization, writing – original draft, writing – review & editing. WCKD: conceptualization, data curation, formal analysis, investigation, methodology, validation, writing – review & editing. TJ: data curation, formal analysis, investigation, methodology, writing – original draft, writing – review and editing. SD: data curation, methodology, writing – review and editing. GZ: conceptualization, supervision, writing – review and editing. ASA: writing, review, editing CSB: conceptualization, funding acquisition, project administration, resources, supervision, writing, review, editing.

Conflicts of interest

There are no conflicts of interest to declare.

Acknowledgements

Funding for this work was provided by the National Science Foundation CAREER Award #1452613.

References

1 K. Milferstedt, W. C. Kuo-Dahab, C. S. Butler, J. Hamelin, A. S. Abouhend, K. Stauch-White, A. McNair, C. Watt, B. I. Carbajal-González, S. Dolan and C. Park, The importance of filamentous cyanobacteria in the development of oxygenic photogranules, *Sci. Rep.*, 2017, **7**, 17944.

2 A. S. Abouhend, A. McNair, W. C. Kuo-Dahab, C. Watt, C. S. Butler, K. Milferstedt, J. Hamelin, J. Seo, G. J. Gikonyo, K. M. El-Moselhy and C. Park, The Oxygenic Photogranule Process for Aeration-Free Wastewater Treatment, *Environ. Sci. Technol.*, 2018, **52**, 3503–3511.

3 A. A. Ansari, A. A. Ansari, A. S. Abouhend, J. G. Gikonyo and C. Park, Photogranulation in a Hydrostatic Environment Occurs with Limitation of Iron, *Environ. Sci. Technol.*, 2021, **55**, 10672–10683.

4 W. C. Kuo-Dahab, K. Stauch-White, C. S. Butler, G. J. Gikonyo, B. Carbajal-González, A. Ivanova, S. Dolan and C. Park, Investigation of the Fate and Dynamics of Extracellular Polymeric Substances (EPS) during Sludge-Based Photogranulation under Hydrostatic Conditions, *Environ. Sci. Technol.*, 2018, **52**, 10462–10471.

5 J. G. Gikonyo, A. S. Abouhend, A. Keyser, Y. Li and C. Park, Scaling-up of oxygenic photogranular system in selective-CSTR, *Bioresour. Technol. Rep.*, 2023, **23**, 101523.

6 A. S. Abouhend, J. G. Gikonyo, M. Patton, C. S. Butler, J. Tobiason and C. Park, Role of Hydrodynamic Shear in the Oxygenic Photogranule (OPG) Wastewater Treatment Process, *ACS ES&T Water*, 2023, **3**, 659–668.

7 A. A. Ansari, A. S. Abouhend and C. Park, Effects of seeding density on photogranulation and the start-up of the oxygenic photogranule process for aeration-free wastewater treatment, *Algal Res.*, 2019, **40**, 101495.

8 M. A. Borowitzka and L. J. Borowitzka, *Micro-algal Biotechnology*, Cambridge University Press, 1988.

9 K. Stauch-White, V. N. Srinivasan, W. Camilla Kuo-Dahab, C. Park and C. S. Butler, The role of inorganic nitrogen in successful formation of granular biofilms for wastewater treatment that support cyanobacteria and bacteria, *AMB Express*, 2017, **7**, 146.

10 L. Delgadillo-Mirquez, F. Lopes, B. Taidi and D. Pareau, Nitrogen and phosphate removal from wastewater with a mixed microalgae and bacteria culture, *Biotechnol. Rep.*, 2016, **11**, 18–26.

11 J. G. Gikonyo, A. Ansari, C. Park and J. Tobiason, Physical characterization of oxygenic photogranules, *Biochem. Eng. J.*, 2022, **186**, 108592.

12 A. A. Ansari, A. A. Ansari, A. H. Khoja, G. J. Gikonyo, A. S. Abouhend and C. Park, The fate and dynamics of iron during the transformation of activated sludge into oxygenic photogranules (OPGs) under hydrodynamic batch conditions for environmental applications, *J. Environ. Chem. Eng.*, 2022, **10**, 108190.

13 J. G. Gikonyo, A. A. Ansari, A. S. Abouhend, J. E. Tobiason and C. Park, Hydrodynamic granulation of oxygenic

photogranules, *Environ. Sci.: Water Res. Technol.*, 2021, **7**, 427–440.
14 A. S. Abouhend, K. Milferstedt, J. Hamelin, A. A. Ansari, C. Butler, B. I. Carbajal-González and C. Park, Growth Progression of Oxygenic Photogranules and Its Impact on Bioactivity for Aeration-Free Wastewater Treatment, *Environ. Sci. Technol.*, 2020, **54**, 486–496.
15 K. Stauch-White, *The Role of Nitrification and Denitrification in Successful Cultivation of Oxygenic Photogranules for Wastewater Treatment*, University of Massachusetts, Amherst, 2016.
16 R. Kumar and V. P. Venugopalan, Development of self-sustaining phototrophic granular biomass for bioremediation applications, *Curr. Sci.*, 2015, **108**, 9.
17 W. Huang, B. Li, C. Zhang, Z. Zhang, Z. Lei, B. Lu and B. Zhou, Effect of algae growth on aerobic granulation and nutrients removal from synthetic wastewater by using sequencing batch reactors, *Bioresour. Technol.*, 2015, **179**, 187–192.
18 L. Liu, H. Fan, Y. Liu, C. Liu and X. Huang, Development of algae-bacteria granular consortia in photo-sequencing batch reactor, *Bioresour. Technol.*, 2017, **232**, 64–71.
19 J. S. M. Ahmad, W. Cai, Z. Zhao, Z. Zhang, K. Shimizu, Z. Lei and D.-J. Lee, Stability of algal-bacterial granules in continuous-flow reactors to treat varying strength domestic wastewater, *Bioresour. Technol.*, 2017, **244**, 225–233.
20 O. Tiron, C. Bumbac, E. Manea, M. Stefanescu and M. Nita Lazar, Overcoming Microalgae Harvesting Barrier by Activated Algae Granules, *Sci. Rep.*, 2017, **7**, 4646.
21 Z. Li, J. Wang, W. Liu, Y. Zhao, Z. Lei, T. Yuan, K. Shimizu, Z. Zhang and D.-J. Lee, Photosynthetic oxygen-supported algal-bacterial aerobic granular sludge can facilitate carbon, nitrogen and phosphorus removal from wastewater: Focus on light intensity selection, *Bioresour. Technol.*, 2023, **388**, 129752.
22 V. Körstgens, H. C. Flemming, J. Wingender and W. Borchard, Uniaxial compression measurement device for investigation of the mechanical stability of biofilms, *J. Microbiol. Methods*, 2001, **46**, 9–17.
23 H. Yin, *Size Kinetics and Mechanics of Clay-biopolymer Flocs*, Louisiana State University and Agricultural and Mechanical College, LSU Doctoral dissertations, 2013, DOI: **10.31390/gradschool_dissertations.3474**.
24 G. Zhang, H. Yin and D. J. Degroot, Thixotropism of micron-sized saltwater clay flocs, *Géotech. Lett.*, 2013, **3**, 162–165.
25 W. Weibull, A Statistical Distribution Function of Wide Applicability, *J. Appl. Mech.*, 2021, **18**, 293–297.
26 Y. Huang, X. Dong, M. Li, M. Zhang and Y. Yu, Density Functional Theory study of the structural and electronic properties of H3PO4/ZSM-5, *RSC Adv.*, 2014, **4**, 14573–14581.
27 American Public Health Association, American Water Works Association and Water Environment Federation, *Standard Methods for the Examination of Water & Wastewater*, ed. E. W. Rice, R. B. Baird and A. D. Eaton, Washington, 23rd edn, 2017.
28 M. DuBois, K. A. Gilles, J. K. Hamilton, P. A. Rebers and F. Smith, Colorimetric Method for Determination of Sugars and Related Substances, *Anal. Chem.*, 1956, **28**, 350–356.
29 B. Frølund, R. Palmgren, K. Keiding and P. H. Nielsen, Extraction of extracellular polymers from activated sludge using a cation exchange resin, *Water Res.*, 1996, **30**, 1749–1758.
30 C. Park and J. T. Novak, Characterization of activated sludge exocellular polymers using several cation-associated extraction methods, *Water Res.*, 2007, **41**, 1679–1688.
31 B. Frølund, T. Griebe and P. H. Nielsen, Enzymatic activity in the activated-sludge floc matrix, *Appl. Microbiol. Biotechnol.*, 1995, **43**, 755–761.
32 O. H. Lowry, N. J. Rosebrough, A. L. Farr and R. J. Randall, Protein measurement with the Folin phenol reagent, *J. Biol. Chem.*, 1951, **193**, 265–275.
33 *R Core Team*, 2022.
34 F. A. Dahalan, N. Abdullah, A. Yuzir, G. Olsson, Salmiati, M. Hamdzah, M. F. M. Din, S. A. Ahmad, K. A. Khalil, A. N. Anuar, Z. Z. Noor and Z. Ujang, A proposed aerobic granules size development scheme for aerobic granulation process, *Bioresour. Technol.*, 2015, **181**, 291–296.
35 Y.-Q. Liu, Y. Liu and J.-H. Tay, Relationship between size and mass transfer resistance in aerobic granules, *Lett. Appl. Microbiol.*, 2005, **40**, 312–315.
36 A. Li, X. Li and H. Yu, Effect of the food-to-microorganism (F/M) ratio on the formation and size of aerobic sludge granules, *Process Biochem.*, 2011, **46**, 2269–2276.
37 F. Rossi and R. De Philippis, Role of Cyanobacterial Exopolysaccharides in Phototrophic Biofilms and in Complex Microbial Mats, *Life*, 2015, **5**, 1218–1238.
38 A. A. Ansari, A. A. Ansari, J. G. Gikonyo, A. S. Abouhend and C. Park, The Coupled Effect of Light and Iron on the Photogranulation Phenomenon, *Environ. Sci. Technol.*, 2023, **57**, 9086–9095.
39 B. S. McSwain, R. L. Irvine, M. Hausner and P. A. Wilderer, Composition and Distribution of Extracellular Polymeric Substances in Aerobic Flocs and Granular Sludge, *Appl. Environ. Microbiol.*, 2005, **71**, 1051–1057.
40 T. Seviour, N. Derlon, M. S. Dueholm, H.-C. Flemming, E. Girbal-Neuhauser, H. Horn, S. Kjelleberg, M. C. M. van Loosdrecht, T. Lotti, M. F. Malpei, R. Nerenberg, T. R. Neu, E. Paul, H. Yu and Y. Lin, Extracellular polymeric substances of biofilms: Suffering from an identity crisis, *Water Res.*, 2019, **151**, 1–7.
41 M. Basuvaraj, J. Fein and S. N. Liss, Protein and polysaccharide content of tightly and loosely bound extracellular polymeric substances and the development of a granular activated sludge floc, *Water Res.*, 2015, **82**, 104–117.
42 A. Melo, C. Quintelas, E. C. Ferreira and D. P. Mesquita, The Role of Extracellular Polymeric Substances in Micropollutant Removal, *Front. Chem. Eng.*, 2022, **4**, 778469.
43 G. Gonzalez-Gil and C. Holliger, Aerobic Granules: Microbial Landscape and Architecture, Stages, and Practical Implications, *Appl. Environ. Microbiol.*, 2014, **80**, 3433–3441.

44 S. Yuan, M. Gao, H. Ma, M. Z. Afzal, Y.-K. Wang, M. Wang, H. Xu, S.-G. Wang and X.-H. Wang, Qualitatively and quantitatively assessing the aggregation ability of sludge during aerobic granulation process combined XDLVO theory with physicochemical properties, *J. Environ. Sci.*, 2018, **67**, 154–160.

45 J. T. Novak, N. G. Love, M. L. Smith and E. R. Wheeler, The effect of cationic salt addition on the settling and dewatering properties of an industrial activated sludge, *Water Environ. Res.*, 1998, **70**, 984–996.

46 F. Kara, G. C. Gurakan and F. D. Sanin, Monovalent cations and their influence on activated sludge floc chemistry, structure, and physical characteristics, *Biotechnol. Bioeng.*, 2008, **100**, 231–239.

47 S. Felz, H. Kleikamp, J. Zlopasa, M. C. M. van Loosdrecht and Y. Lin, Impact of metal ions on structural EPS hydrogels from aerobic granular sludge, *Biofilm*, 2020, **2**, 100011.

48 M. J. Higgins and J. T. Novak, The effect of cations on the settling and dewatering of activated sludges: Laboratory results, *Water Environ. Res.*, 1997, **69**, 215–224.

49 S. C. Lachmann, T. Mettler-Altmann, A. Wacker and E. Spijkerman, Nitrate or ammonium: Influences of nitrogen source on the physiology of a green alga, *Ecol. Evol.*, 2019, **9**, 1070–1082.

50 X. Ran, X. Zhang, B. Zhao and Q. An, Unraveling the two-sided effect of nitrate on aerobic granulation, *Chem. Eng. J.*, 2024, **479**, 147430.

51 J. Wan and M. Sperandio, Possible role of denitrification on aerobic granular sludge formation in sequencing batch reactor, *Chemosphere*, 2009, **75**, 220–227.

52 M. Lürling, M. M. E. Mello, F. van Oosterhout, L. de Senerpont Domis and M. M. Marinho, Response of Natural Cyanobacteria and Algae Assemblages to a Nutrient Pulse and Elevated Temperature, *Front. Microbiol.*, 2018, **9**, 1851.

53 W. Gongi, J. L. Gomez Pinchetti, N. Cordeiro and H. B. Ouada, Extracellular Polymeric Substances Produced by the Thermophilic Cyanobacterium Gloeocapsa gelatinosa: Characterization and Assessment of Their Antioxidant and Metal-Chelating Activities, *Mar. Drugs*, 2022, **20**, 227.

54 R. D. Robarts and T. Zohary, Temperature effects on photosynthetic capacity, respiration, and growth rates of bloom-forming cyanobacteria, *N. Z. J. Mar. Freshwater Res.*, 1987, **21**, 391–399.

55 C. Wang and C. Q. Lan, Effects of shear stress on microalgae - A review, *Biotechnol. Adv.*, 2018, **36**, 986–1002.

56 D. G. Adams, D. Ashworth and B. Nelmes, Fibrillar Array in the Cell Wall of a Gliding Filamentous Cyanobacterium, *J. Bacteriol.*, 1999, **181**, 884–892.

57 E. Hoiczyk and A. Hansel, Cyanobacterial Cell Walls: News from an Unusual Prokaryotic Envelope, *J. Bacteriol.*, 2000, **182**, 1191–1199.

58 V. Körstgens, H. C. Flemming, J. Wingender and W. Borchard, Influence of calcium ions on the mechanical properties of a model biofilm of mucoid Pseudomonas aeruginosa, *Water Sci. Technol.*, 2001, **43**, 49–57.

59 Y. Wang, J. Wang, Z. Liu, X. Huang, F. Fang, J. Guo and P. Yan, Effect of EPS and its forms of aerobic granular sludge on sludge aggregation performance during granulation process based on XDLVO theory, *Sci. Total Environ.*, 2021, **795**, 148682.

60 P. Di Martino, Extracellular polymeric substances, a key element in understanding biofilm phenotype, *AIMS Microbiol.*, 2018, **4**, 274–288.

61 Y. M. Lin, P. K. Sharma and M. C. M. van Loosdrecht, The chemical and mechanical differences between alginate-like exopolysaccharides isolated from aerobic flocculent sludge and aerobic granular sludge, *Water Res.*, 2013, **47**, 57–65.